Taylor & Francis
Taylor & Francis Group

Molecular Crystals and Liquid Crystals

ISSN: 1542-1406 (Print) 1563-5287 (Online) Journal homepage: http://www.tandfonline.com/loi/gmcl20

Analysis on electron emission characteristics of MgO layer with MgO crystal powder under various panel temperatures in ac-plasma display panels

Jae Hyun Kim, Hyung Dal Park, Choon-Sang Park, Hyun-Jin Kim, Bhum Jae Shin, Jeong Hyun Seo & Heung-Sik Tae

To cite this article: Jae Hyun Kim, Hyung Dal Park, Choon-Sang Park, Hyun-Jin Kim, Bhum Jae Shin, Jeong Hyun Seo & Heung-Sik Tae (2017) Analysis on electron emission characteristics of MgO layer with MgO crystal powder under various panel temperatures in ac-plasma display panels, Molecular Crystals and Liquid Crystals, 645:1, 102-111, DOI: 10.1080/15421406.2016.1277489

To link to this article: https://doi.org/10.1080/15421406.2016.1277489

Published online: 10 May 2017.

MOLECULAR CRYSTALS AND LIQUID CRYSTALS
2017, VOL. 645, 102–111
http://dx.doi.org/10.1080/15421406.2016.1277489

Taylor & Francis
Taylor & Francis Group

Analysis on electron emission characteristics of MgO layer with MgO crystal powder under various panel temperatures in ac-plasma display panels

Jae Hyun Kim[a], Hyung Dal Park[b], Choon-Sang Park[c], Hyun-Jin Kim[c], Bhum Jae Shin[d], Jeong Hyun Seo[e], and Heung-Sik Tae[c]

[a]Radiation Instrumentation Research Division, Korea Atomic Energy Research Institute, Jeongeup, Jeollabuk-do, South Korea; [b]Radiation Technology eXcellence (RTX), Daejeon, Korea; [c]School of Electronics Engineering, College of IT Engineering, Kyungpook National University, Daegu, South Korea; [d]Department of Electronics Engineering, Sejong University, Seoul, South Korea; [e]Department of Electronics Engineering, University of Incheon, Incheon, South Korea

ABSTRACT

This paper examines the electron emission characteristics of the MgO layer in the case of spraying the MgO crystal powders based on the two monitoring parameters such as the electric field strength and the panel temperature. In particular, in order to analyze the effects of the electric field strength on the electron emission characteristics of the MgO layer with MgO crystal powders, the variations in the wall voltage induced by the electron emission are measured relative to the electric field strength between the address-sustain electrodes during an address period under various panel temperature conditions ranging from −5 to 65°C. As a result, it is observed that the electron emission characteristics of the MgO layer with MgO crystal powder strongly depend on the electric field strength rather than the thermal effect of exo-electron emission, which is confirmed by the measurement result of the wall voltage variation relative to the electric field strength under the low panel temperature of −5°C.

KEYWORDS

LED; light extraction; patterned surface; Ga-doped ZnO

1. Introduction

An MgO protective layer in ac-plasma display panels (PDPs) plays an important role in producing a stable discharge by lowering the firing voltage thanks to its high secondary electron emission coefficient. As the sizes of PDPs are becoming larger and their cell numbers are increasing considerably, the importance of address discharge is more emphasized under the address-display-separated (ADS) driving method, thereby requiring better performance of the MgO layer. In particular, fast address discharge characteristics of the MgO layer are required [1–3]. Furthermore, the fast address discharge characteristics of the MgO layer should be maintained under various panel temperatures. However, the conventional MgO protective layer is very sensitive to variation in the panel temperature, meaning that the address discharge characteristics are quite different depending on the panel temperature. That is, in the case of the conventional MgO layer, the address discharge tends to vary very

CONTACT Heung-Sik Tae hstae@ee.knu.ac.kr
Color versions of one or more of the figures in the article can be found online at www.tandfonline.com/gmcl.

unstably depending on the variation in the panel temperature [4, 5]. Recently, in order to compensate the demerits of conventional MgO layers, various types of MgO crystal powders have been used as functional layers to improve the address delay characteristics [6–12], and simultaneously to lower the firing voltage in mini-test panels as a consequence of high priming electron by exo-electron emission [13–17]. However, the detailed mechanism of electron emission from the MgO crystal powders has not been clarified yet.

Therefore, in this paper, to analyze the effects of the electric field on the electron emission characteristics of the MgO layer with MgO crystal powders, the variations in the wall voltage induced by the electron emissions are measured relative to the electric field strength between the address (A)-scan (Y) electrodes during an address period, and the corresponding electron emission mechanism of MgO crystal powders is discussed based on the changes in the electron emission affected by the electric field intensity.

2. Experimental setup

Figures 1 (a) and (b) show the SEM images of the conventional MgO layer without MgO crystal powders and the MgO layer with MgO crystal powders used in this study, respectively. In both cases, the MgO layer was deposited by using the ion-plating method and its thickness was 6500 Å [18]. The MgO crystal powder (20 wt %) was coated on the MgO layer by using the spray method. The F-doped MgO crystal powders were manufactured by using a vapor-phase oxidation method in which the fluorine was doped into MgO crystal powder by additionally injecting SF_6 gas to the reaction chamber. As a result, an O^{2-} in the crystal structure of the MgO powder was replaced by a F^{1-}, so that the MgF_2 existed in the MgO crystal powder. Consequently, the electron traps to facilitate the electron emissions in micro-discharge cells were able to be established below the conduction band of the MgO layer [19]. The F-doped MgO crystals illustrated the various grain sizes with cubic structures ranging from tens of nanometers to a few micrometers, as shown in the SEM image of the F-doped MgO crystal powder of Fig. 1 (b).

Figure 2 (a) shows the optical-measurement system and 6-inch test panel with three electrodes employed in this experiment, where X is the sustain electrode, Y is the scan electrode, and A is the address electrode. The cell size of the 6-inch test panel was a 42-inch HD grade. An ultra driving system (UDS) and photo-sensor amplifier (Hamamatsu, C6386) were used to measure the address delay time and the variation in the wall voltage. The panel

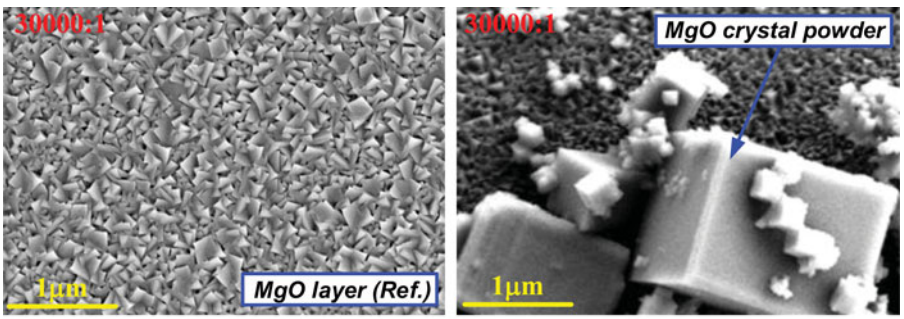

Figure 1. Comparison of SEM images of MgO layer (a) without and (b) with MgO crystal powders.

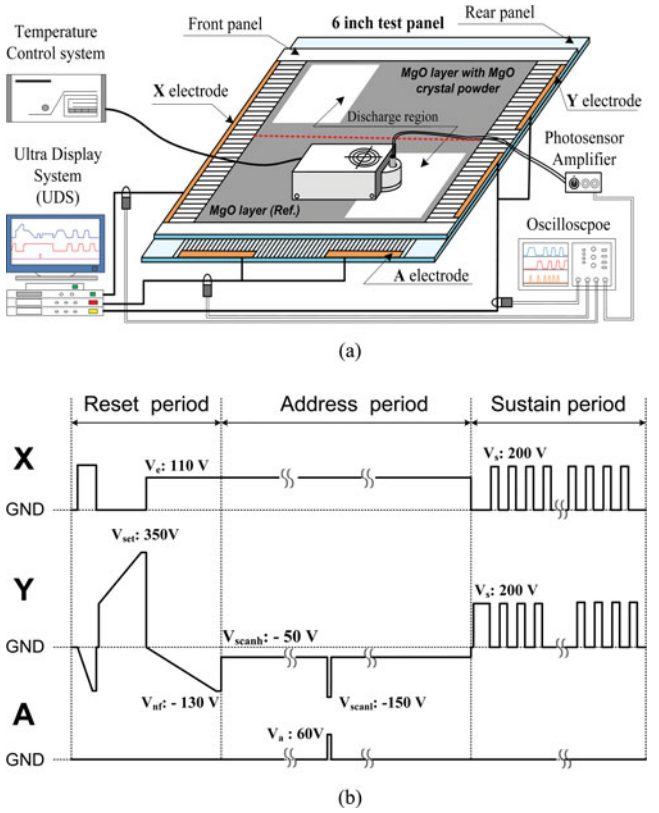

Figure 2. Schematic diagrams of (a) measurement system and (b) driving waveform used in this study.

temperature of the test panel was varied from −5 to 65°C by controlling the temperature (Acetec, CU3940) on the glass of the front panel with an external cooler and heater. The gas chemistry in the test panel was Ne-Xe (17%)-He (35%) under a pressure of 420 Torr. The MgO layer in the upper part of the test panel was coated by the MgO crystal powders shown in Fig. 1 (b), whereas the MgO layer in the lower part of the test panel had no MgO crystal powders. The detailed specifications of the upper and lower parts of the test panel were exactly same, except for the MgO crystal powders, as shown in Table 1.

Fig. 2 (b) shows the conventional driving waveforms, including the reset, address, and sustain-periods. As shown in Fig. 2 (b), the address voltage (=V_a) of 60 V, the scan high voltage (=V_{scanh}) of −50 V, and the scan low voltage (=V_{scanl}) of −150 V were applied during the address -period, whereas the sustain voltage of 200 V was applied under a driving frequency of 200 kHz during the sustain-period.

Table 1. Specifications of 6-in. test ac-PDP employed in this study.

Front panel		Rear panel	
ITO width	220 μm	Barrier rib width	60 μm
ITO gap	70 μm	Barrier rib height	120 μm
Bus width	50 μm	Address width	90 μm
Cell pitch		912 μm X 692 μm	
Gas pressure		420 Torr	
Gas chemistry		Ne-He(35%)-Xe(17%)	
Panel temperature		−5°C ~ + 65°C	

3. Results and discussion

3.1. Characteristics of address delay time under variable panel temperature

Figures 3 (a) and (b) show the changes in the address discharge delay times relative to the panel temperature. In both cases of MgO layers without and with MgO crystal powders, the formative delay time (*i.e.*, T_f) was increased with a decrease in the panel temperature. However, for the statistical delay time (*i.e.*, T_s), there are very different tendencies for the various panel temperatures, especially in the case of low panel temperature (−5°C).

It is well known that the T_s is influenced by the number of seed electrons supplied to the discharge space, which is called as priming particles, and as such the value of T_s is determined by the following equation (1);

$$T_s = \frac{1}{n_0 P_s} \tag{1}$$

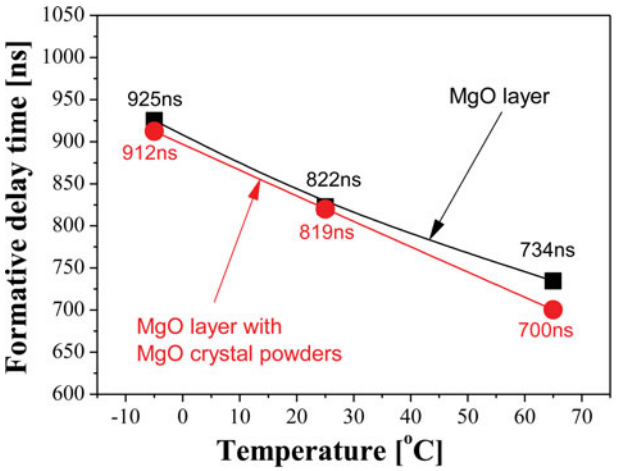

Figure 3. Changes in the (a) formative and (b) statistical delay time under various panel temperatures from −5°C to 65°C from 6-in. test panel without and with MgO crystal powders.

where n_0 is the number of seed electrons and P_s is the probability of an avalanche. Thus, the T_s is inversely proportional to the concentration of seed electrons. Theses seed electrons are supplied through exo-electron emissions from the MgO surface during the address-period [16]. In general, it is well known that the amount of the exo-electrons emitted from the MgO surface is significantly affected by the panel temperature. In particular, at a high panel temperature, the exo-electron emissions increase due to the thermal activation, thus resulting in inducing the decrease of the statistical delay time, T_s. In contrast, at a low panel temperature, the statistical delay time considerably increases due to the decrease of the exo-electron emission, which is closely related to the amount of the seed electrons in the discharge space [9, 14–17].

As shown in Fig. 3 (b), for the MgO layer without MgO crystal powders, the statistical delay time, T_s was increased with a decrease in the panel temperature. In particular, the statistical delay time, T_s was dramatically increased at a low temperature (−5°C), and such an increase would be caused by the reduced thermal activation. However, for the MgO layer with MgO crystal powders, the statistical delay time, T_s was almost the same irrespective of the variations in the panel temperature. This drastic reduction in the variation of the statistical delay time in the case of adopting the MgO layer with MgO crystal powders means no variations in the amounts of seed electrons irrespective of the panel temperature variation. Thus, the application of the MgO crystal powder could minimize the dependence of the exo-electron emission on the panel temperature. Consequently, this experimental result implies that another factor, for example, the electric field effect instead of the thermal effect, could be considered in investigating what factor would be dominant for facilitating the emission of exo-electrons from the MgO surface with MgO crystal powders especially under a low panel temperature (*i.e.*, −5°C).

3.2. Characteristics of cathodoluminescence

Figure 4 shows the schematic diagram of the cathodoluminescence (CL) measurement system for analyzing and comparing the electron emission characteristics from the defect and trap levels of both the MgO layer without MgO crystal powders (=reference MgO layer) and the MgO layer with MgO crystal powders, respectively. The electron emission characteristics at the defect and trap levels of each sample can be obtained by the following process. As shown in Fig. 4, when the samples are scanned by the electron beam from the electron-beam

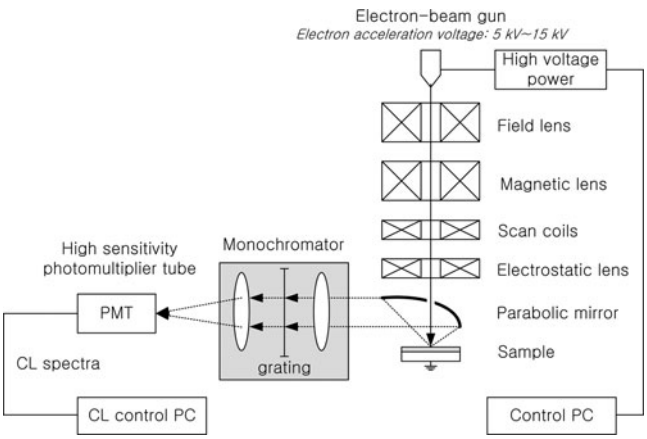

Figure 4. Schematic diagram of cathodoluminecence measurement system.

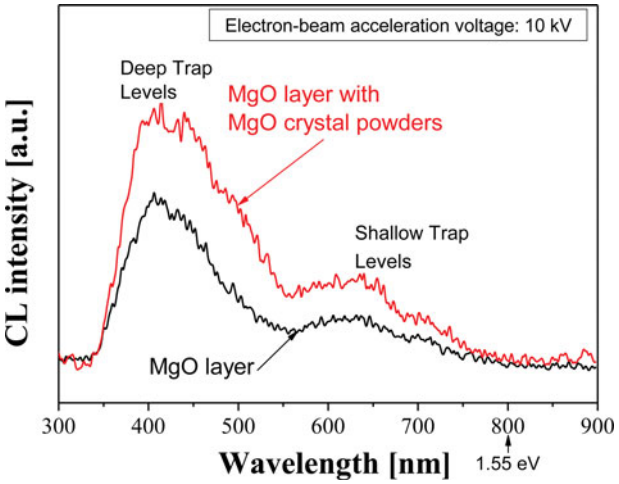

Figure 5. Changes in CL intensity of MgO layer without MgO crystal powders and MgO layer with MgO crystal powders under electron acceleration voltage (10 kV) condition.

gun, the emission of light from the samples occurs due to the electron excitation across the band gap and its corresponding transition. This light is collected by the PMT through the monochromator and transformed to the cathodoluminescence spectrum [20, 21].

Figure 5 shows the CL intensities of the reference MgO layer and the MgO layer with MgO crystal powders measured from the CL measurement system of Fig. 4 at an electron beam acceleration voltages of 10 kV. As shown in Fig. 5, the CL intensity of MgO layer with MgO crystal powders was greater than that of the reference MgO layer, especially at the deep trap level ranging from 390 to 530 nm and shallow trap level ranging from 600 to 800 nm. The increased CL intensity of the MgO layer with MgO crystal powder are presumably induced by the increased impurity level (*i.e.* the electron trap level) due to the fluorine doped into the MgO crystal powders. In addition, these CL intensities at two ranges, the deep and shallow trap levels, are closely related to the amount of electrons emitted from the MgO layer into the discharge space [17]. Thus, the overall decreases in the formative and statistical delay times in Figs. 3 (a) and (b) seem to be in accordance with an increase of the CL intensities at both the deep and shallow trap levels. Nonetheless, the drastic reduction of the statistical delay time even at a low temperature in Fig. 4 (b) is not easily explained by the increase of the electron emission due to the increased impurity level. Therefore the additional monitoring of the panchromatic CL image under various electron beam acceleration voltages is needed to investigate whether the electron emission characteristics are related to the intensity of electric field applied to the MgO crystal powder.

Figure 6 shows the changes in the panchromatic CL image under various electron beam acceleration voltages ranging from 5 to 15 kV. A panchromatic CL image can show the two-dimensional spatial distribution of the cathodoluminescence from the sample. For the panchromatic CL images of the MgO layer with MgO crystal powder in Fig. 6 (a), the CL images were captured by focusing the electron beam toward the center of the MgO single crystal powder. In the panchromatic image of Fig. 6, the bright and dark parts mean the relative values of the electron emissions. As shown in Fig. 6 (b), for the reference MgO protective layer, the electron emissions were slightly increased with respect to the increased electron beam acceleration voltage. However, for the MgO layer with the MgO crystal powder, the brightness difference between the MgO single crystal powder and MgO layer is increased

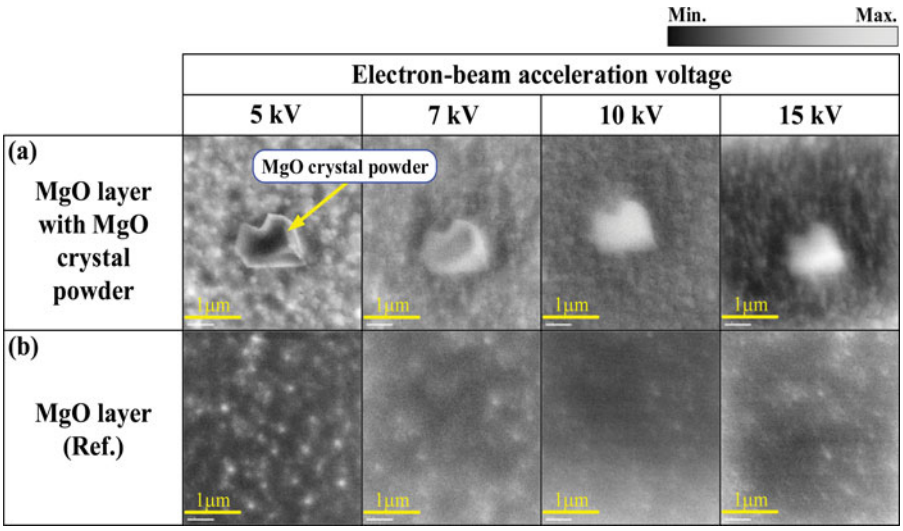

Figure 6. Changes in panchromatic CL image under various electron beam acceleration voltages.

with respect to the increased electron beam acceleration voltage, as shown in Fig. 6 (a). In particular, at the low electron beam acceleration voltage, the brightest parts were distributed along the edge of the MgO crystal powder. Meanwhile, at a high electron beam acceleration voltage, the electron emissions were more intensified and extended to the surface of the MgO crystal powder. This strong dependence of the electron emissions on the electron beam acceleration voltages especially for the MgO layer with MgO crystal powders is presumably related to the strong electric field at the edge of the MgO crystal powder and the corresponding increase in the electron emissions at the edge region. Furthermore, since the amount of electron emissions from the MgO crystal powder under high electron beam acceleration voltage was much larger than those from the MgO layer under low electron beam acceleration voltage, the overall electron emission characteristics in the case of the MgO layer with MgO crystal powder would be mainly determined by the amplitude of the voltage applied to the discharge space with a lower dependence on the variation of the panel temperature. In particular, it is expected that the high intensive electric field can be generated even at an applied voltage of 100–200 V in the discharge space of the PDP cells because the dimension of the PDP cell is in a range of one hundred micrometer (*i.e.*, barrier rib height is 120 μm). Also, in the microcells of the PDP, this dependence of the electron emission on the applied voltage would be more effective for the electrons released from the shallow trap levels than the electrons released from the deep trap levels, because the transition energy from the shallow trap levels to the conduction band is much lower than those from the deep trap levels [22]. Considering that the amount of the electron emission from the shallow trap level affects easily the changes of the statistical delay time [17], the inferences discussed above could explain the drastic reduction of the statistical delay time at a low temperature in Fig. 4 (b).

3.3. Wall voltage variation relative to electric field strength between A-Y electrodes

In order to analyze the effects of the electron emission characteristics of the MgO layer with MgO crystal powder in Figs. 5 and 6, the variations in the wall voltage induced by the exo-electron emission were measured relative to the electric field strength between the A-Y electrodes during an address period without producing the address discharge under various panel

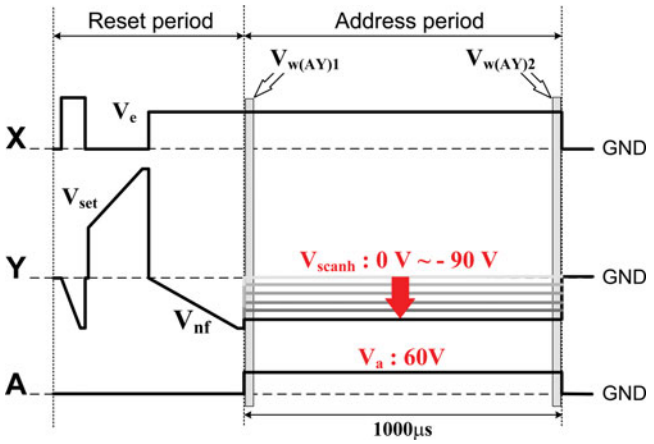

Figure 7. Driving waveform employed for measuring wall voltage variations during address-period relative to electric field strength between A-Y electrodes.

temperature conditions. Figure 7 shows the driving waveform employed to measure the electron emission characteristics of the MgO protective layer with and without MgO crystal powders depending on the variation in the electric field strength. The wall voltage variation between the A and Y electrodes, defined by $|V_w(AY)1\text{-}V_w(AY)2|$, measured the wall voltage formed through the reset discharge ($V_w(AY)1$) and the wall voltage change during the address period ($V_w(AY)2$); the V_{scanh} voltage was varied from 0 to −90 V in order to investigate only the electron emission phenomenon without producing the address discharge [23]. Other voltages during the address period are fixed as follows: X-bias voltage (V_e) was 110 V, V_{nf} was −130 V, and address voltage (V_a) was 60 V. The total voltage difference between the A-Y electrodes was changed from 60 V to 150 V, as shown in Table 2.

Figure 8 shows the variations of wall voltages relative to the electric field strength between the A-Y electrodes under the reference MgO layer for three different panel temperatures such as −5°C, 20°C, and 65°C, respectively. In cases of the reference MgO layer, with an increase of the panel temperature from −5 to +65°C, the wall voltage variation relative to electric field strength was gradually increased, which would be caused mainly by the thermal effect.

Figure 9 show the variations of wall voltages relative to the electric field strength between the A-Y electrodes under the MgO layer with the MgO crystal powder for three different panel temperatures such as −5°C, 20°C, and 65°C, respectively. In the case of the MgO protective layer with the MgO crystal powders, however the wall voltage variation was almost the same, as shown in Fig. 9, irrespective of the variations in the panel temperatures, meaning that the electron emission characteristics of the MgO protective layer with the MgO crystal powders strongly depend on the electric field strength instead of the thermal electron emission. These

Table 2. Various applied voltage levels employed in driving waveform in Fig. 7.

Applied voltage	
V_{set}	350 V
V_e	110 V
V_{nf}	130 V
V_a	60 V
V_{scanh}	0 V ~ −90 V
Total changed electric field strength between A-Y electrodes during address period	60 V ~ 150 V
Panel temperature	−5°C ~ +65°C

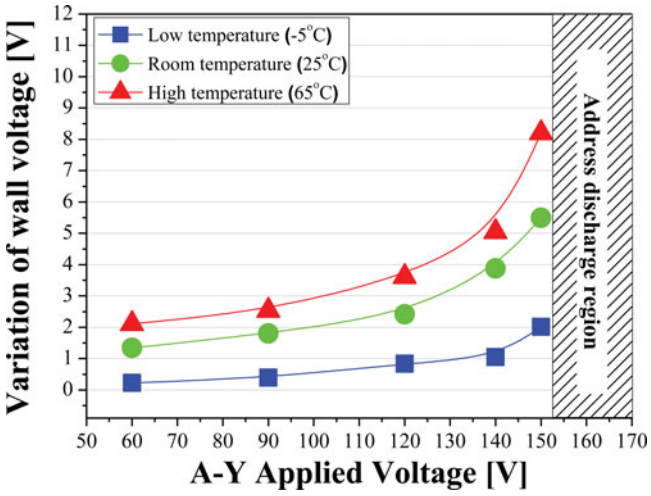

Figure 8. Variations of wall voltage relative to electric field strength between A-Y electrodes under various panel temperatures in case of adopting MgO layer without MgO crystal powders.

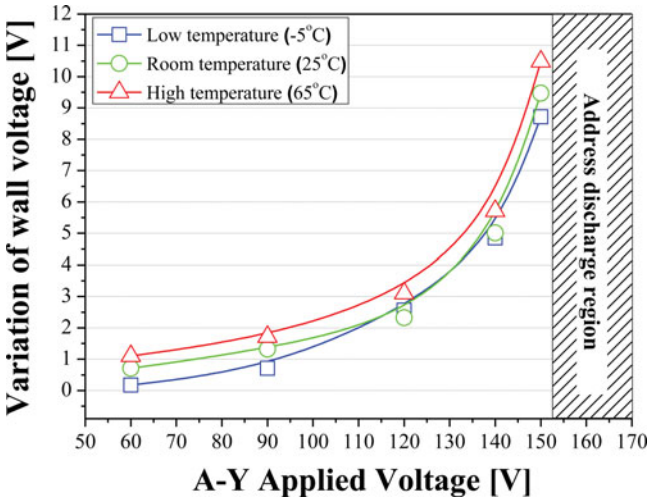

Figure 9. Variations of wall voltage relative to electric field strength between A-Y electrodes under various panel temperatures in case of adopting MgO layer with MgO crystal powders.

results indicate that the electric field emission would more important factor than the thermal electron emission in the case of the MgO layer with MgO crystal powders.

4. Conclusions

In this paper, to analyze the effects of the electric field strength on the electron emission characteristics of the MgO layer with MgO crystal powders, the variations in the wall voltage induced by the electron emissions were measured relative to the electric field strength between the A-Y electrodes during address period. The experimental results showed that the exo-electron emission of the MgO layer without MgO crystal powders was related to the thermal effect relative to panel temperature, whereas the exo-electron emission of the MgO layer with MgO crystal powders was related to the electric field strength rather than the thermal effect relative to the panel temperatures. Finally, spraying the MgO crystal powders on the

MgO layer can contribute to minimizing the variations in the electron emission characteristics with the panel temperature, especially a low panel temperature.

Funding

This work was supported by the National Research Foundation of Korea (NRF) grant funded by the Korea government (MOE) (No. 2016R1D1A1B03933162).

References

[1] Boeuf, J. P. (2003). *J. Phys. D: Appl. Phys.*, *36*, R53.
[2] Park, C.-H., Lee, S.-H., Kim, D.-H., Lee, W.-G., & Heo, H.-E. (2001). *IEEE Trans. Electron Devices*, *48*, 2260.
[3] Kim, J. S., Yang, J. H., Kim, T. J., & Whang, K.–W. (2003). *IEEE Trans. Plasma Sci.*, *31*, 1083.
[4] Ryu, J.-H., Choi, J.-Y., Lee, H.-J., Kim, D.-H., Lee, H. J., & Park, C.-H. (2004). *IEEE Trans. Electron Devices*, *51*, 2026.
[5] Shin, B. J., Choi, K. C., Tae, H.-S., Seo, J. H., Kim, J.-Y., & Han J.-W. (2005). *IEEE Trans. Plasma Sci.*, *33*, 162.
[6] Jung, H.-Y., Lee, T.-H., Kwon, O. K., Cheong, H.-W., Steinmuller, S. O., Janek, J., & Whang, K.-W. (2010). *IEEE Electron Device Lett.*, *31*, 686.
[7] Kim, R. H., Kim, Y. H., Cho, J. H., & Park, J.-W. (2000). *J. Vac. Sci. Technol. A*, *18*, 2493.
[8] Choi, J.-S., Moon, S.-H., Kim, J.-H., & Kim, G.-H. (2010). *Curr. Appl. Phys.*, *10*, 1378.
[9] Okada, T. & Yoshioka, T. (2008). *Appl. Phys. Lett.*, *93*, 171501.
[10] Kim, J. K. (2013). *IEEE Trans. Electron Devices*, *60*, 2556.
[11] Kim, J. H., Park, C.-S., Park, H. D., Tae, H.-S., & Lee, S.-H. (2013). *J. Nanosci. Nanotechnol.*, *13*, 3270.
[12] Jung, E. Y., Park, C.-S., Hong, T. E. & Sohn, S. H. (2014). *Jpn. J. Appl. Phys.*, *53*, 069203.
[13] Kim, Y.-S., Yoon, S.-H., & Yang, H. (2010). *J. Appl. Phys.*, *107*, 013303.
[14] Yoon, S.-H., Hong, C.-R., Ko, J. J., Yang, H.-S., & Kim, Y.-S. (2009). *J. Soc. Inf. Disp.*, *17*, 131.
[15] Okada, T., Naoi, T., & Yoshioka, T. (2009). *J. Appl. Phys.*, *105*, 113304.
[16] Okada, T., Furutani, T., & Yoshioka, T. (2008). *Appl. Phys. Express*, *1*, 091203.
[17] Motoyama, Y., Hirano, Y., Ishii, K., Murakami, Y., & Sato, F. (2004). *J. Appl. Phys.*, *95*, 8419.
[18] Oumi, K., Matsumoto, H., Kashiwagi, K., & Murayama, Y. (2003). *Surf. Coat. Technol.*, *562*, 169.
[19] Kuang, W.-J., Li, Q., Chen, Y.-X., Hu, K., Wang, N.-H., Xing, F.-L., Yan, Q., Sun, S.-S., Huang, Y., Tao, Y., & Tolner, H. (2013). *J. Phys. D: Appl. Phys.*, *46*, 365501.
[20] Ghamnia, M., Jardin, C., & Bouslama, M. (2003). *J. Electron Spectrosc. Relat. Phenom.*, *133*, 55.
[21] Hirakawa, T. & Uchiike, H. (2003). *in Proc. IDW'03 Dig.*, p. 873.
[22] Rosenblatt, G. H., Rowe, M. W., Williams, G. P., & Williams, R. T. (1989). *Phys. Rev. B*, *39*, 10309.
[23] Jang, S.-K., Park, C.-S., Tae, H.-S., Shin, B. J., Seo, J. H., Jung, , & Jung, E.-Y. (2010). *J. Soc. Inf. Disp.*, *18*, 641.